J. Fluid Mech. (1976), *vol.* 73, *part* 4, *pp.* 693–719
Printed in Great Britain

An experimental study of turbulent convection in air

By DANIEL E. FITZJARRALD
Institute of Geophysics and Planetary Physics, Los Angeles, California 90024†

(Received 23 July 1974 and in revised form 14 October 1975)

An experiment was performed in a 3·5 by 3·5 m variable-height, closed convection box, with conditions ranging from a Rayleigh number of 4×10^4 up to 7×10^9, using air as the working fluid. Heat-flux measurements made at Rayleigh numbers up to 7×10^9 yielded a Nusselt number $Nu = 0{\cdot}13Ra^{0{\cdot}30}$. Velocities and temperatures were measured up to $Ra = 1{\cdot}7 \times 10^7$, and Fourier spectra calculated to find the predominant horizontal scales of the motion midway between the boundaries. The predominant scale at $Ra \sim 10^5$ was approximately four times the distance between plates, changing to six as Ra increased to 10^6. With side walls introduced so that the transverse aspect ratio was equal to five, Fourier spectra indicated considerable smaller scale motions, approximately equal to the layer depth. These motions decreased in size as Ra was increased. The results are discussed in relation to previous experimental and theoretical work.

1. Introduction

The fluid motion providing the vertical transport of heat in a gravitational field is an easily realizable situation in which the governing parameter and turbulent transport are uniform within the domain of interest. With a minimum of experimental parameters, the closed convection box can yield a turbulent flow in which the temporal and spatial characteristics of the motion can be systematically investigated. Many of the important features of turbulent convection in other geometries are exhibited by this flow.

One particular feature of turbulence that has been the subject of numerous recent investigations and will be of interest in the present work is the scale size of observed regular structure. Measurements by Blackwelder & Kovasznay (1972) in a turbulent boundary layer indicate that the predominant scale of motion is much larger than the scale length of the flow.

Transition to turbulence is another area in which thermal convection elucidates processes that are observed in other turbulent flows. Vortex pairing in the development of shear flow, as observed by Browand & Winant (1973), has its analogue in the succession of instabilities that lead to turbulent convection.

There are two directions from which turbulent convection can be approached. We can start from steady flows that are just barely unstable, and proceed through the various states that exist as the governing parameter is increased. Or we can make assumptions about the nature of the flow, and develop bounds on the fully-turbulent state that give rise to certain structures. The former method is based on

† Present address: Wave Propagation Laboratory NOAA, Boulder, Colorado.

the observations of Malkus (1954*a*), who found a series of discontinuities in heat flux indicating that new modes were being generated. Willis & Deardorff (1967), Krishnamurti (1970), Brown (1973), Carroll (1971) and Busse & Whitehead (1974) investigated the structures of these modes in the laboratory. The technique is to proceed step by step, relating measurements of a new transition to the previous state and to physical processes that cause the instability.

The latter method of approaching thermal turbulence is based on the suggestion by Malkus (1954*b*) that the turbulence arranges itself so as to maximize the heat flux between the boundaries. This notion is the physical basis for these bounding theories, and distinguishes them from the more conventional theories based on arbitrary kinematic or stochastic assumptions of isotropy and homogeneity. Howard (1963) and Busse (1969) used this approach, finding upper bounds on the turbulent transport and the structure of possible flows.

The present work is an experimental study of moderate-to-high Rayleigh number convection in air. We begin in the region just above the heat flux discontinuities, and move upward to highly-turbulent flow. In analysing the present results we use both the aforementioned approaches (i.e. we move up from previous workers' results at lower Rayleigh numbers, and we investigate structures in the fully-turbulent flow). The experimental apparatus, which is described in §2, is larger than that used by previous researchers, allowing both higher Rayleigh numbers and larger aspect ratios to be used. In addition, the data-gathering techniques make possible analysis of a greater amount of data.

We begin, after describing the apparatus, by investigating the Rayleigh-number dependence of the heat flux in §3. Section 4 describes the results of measurements of temperature and velocity and their horizontal variation. The influence of Rayleigh number on these variations is explored in detail. In §5 the spectral variation at high Rayleigh number is examined, in an attempt to discern any organized structures that might exist in the flow. Section 6 summarizes the results and relates them to previously reported work.

2. Description of apparatus and data analysis

2.1. *Apparatus*

A variable-height convection box was used for the experiments, with air (Prandtl number 0·71) as the working fluid. The sides of the box were of styrofoam insulation. The top and bottom boundaries of the region consisted of 3·5 m square flat plates formed of sheet aluminium attached to aluminium structural members, with water channels between the structural members to maintain the plates at a given temperature. The water flowed directly across each plate from a large supply manifold along one side, through the water channels to a collection trough on the other side. Water was supplied to the manifolds from two 120 litre reservoirs that were maintained at constant temperatures monitored by means of Cu-Con thermocouples for the duration of each experimental period. The cold reservoir could be maintained between room temperature and 3 °C by means of a 3 h.p. refrigeration unit. The hot reservoir was maintained at between room temperature and 40 °C by use of the hot side of the refrigeration unit or electrical

heaters. The primary method for changing operating conditions was to raise or lower the top surface, since the appropriate dimensionless parameter is the Rayleigh number, which varies as the cube of the gap height, $Ra = gd^3\Delta T/\nu k\bar{T}$. Here d is the distance between the plates; ΔT and $\bar{T}$ are the difference and mean of the plate absolute temperatures; ν is the kinematic viscosity; and k is the thermal diffusivity. The minimum d was 6 cm, because of the construction of the water channels, and the maximum d was 180 cm, because of the laboratory dimensions.

Flow rates through the water channels were kept at approximately 2 l s^{-1}, with the maximum change in temperature between inlet and outlet of any channel being less than 0·3 °C for $\Delta T = 10$ °C. The lower plate was adjusted as nearly as possible to the horizontal using a carpenter's level. The exact angle between the lower plate and the local gravity vector is not known; but it is believed to have been so small that it did not affect the results. No large-scale flow was detected in the chamber under convective conditions. The plates were not exactly flat, with waves between the structural supports. The waviness was visible as reflexions on the surface and had a maximum amplitude of approximately 1 mm. The maximum error in d occurred at the lowest values of d and was believed to be less than 2 %, including both the waviness in the surface of the plates and determination of the separation d. For $d > 14$ cm, the error in determining d was approximately 1 %. Time variation of the temperatures of the plates was less than 1 % for the duration of each experiment. Spatial variation of plate temperature was not determined. However, measurement of the temperature in the different water channels indicated variations to be less than 3 % for the smallest temperature differences.

2.2. *Velocity and temperature measurement*

Wollaston-process platinum wire etched to 2·5 μm was used to measure the horizontal and vertical velocity and temperature. For temperature measurement, a series resistor limited the current to less than 0·75 mA through the 5 mm long (100 Ω at 20 °C) wire. Associated circuitry amplified the voltage across the wire approximately 100 times, and low-pass filtered it to attenuate those frequencies above 20 Hz.

Velocity was measured with two 2·5 mm (50 Ω at 20 °C) wires oriented at $\pm 45°$ from the horizontal. This technique is a standard one; it is discussed in detail by Deardorff & Willis (1967). The wires were maintained at a constant temperature (resistance) by means of a servo circuit. The overheat ratio was kept equal to two, corresponding to a wire temperature of 304 °C. Additional circuitry was built to obtain the sum and difference of the two hot-wire outputs and to low-pass filter the results.

The wire sensors were mounted on 15 mm long steel needles, which in turn were mounted on a 13 cm probe. The hot wires were 2·5 mm apart, and the temperature wire was centred 5 mm above and 3·5 mm in front of the hot wires. The probe was placed on a car designed to traverse along a line through the chamber with minimum vibrations and oscillations (figure 1 (*a*)). It was fastened onto a variable height post 3 cm long, 1 cm wide, and high enough that the probe support was midway between the top and bottom plates. The four-wheeled, rubber-tyred car,

weighted to minimize vibration, was propelled along the lower plate at 28·3 cm s^{-1} by a constant r.p.m. motor, and carried the probe assembly through the working fluid.

Velocity errors due to both vibration and waviness of the lower plate were encountered. The size of these errors depended upon the magnitude of velocities being measured, varying from less than 5% for most of the cases investigated up to approximately 10% for those with the smallest velocities. It should be noted that the spectra of these velocity errors were quite different from spectra of the velocity signal. No fixed-frequency spectral peaks corresponding to the plate waviness were observed in the results, so that low-frequency errors due to the waviness of the lower plate were not significant. Vibrations of the support were of higher frequency than the convective velocities being measured; the highest-frequency velocity analysed below is approximately 5 Hz, below the vibration frequency. Again, no steady spectral peak was observed in the results, indicating that probe vibrations were not significant. The measured spectra to be given below are therefore nearly unaffected by errors due to the traversing mechanism.

When the probe is moving through the fluid, the difference between the crossed hot wires is proportional to the vertical velocity of the fluid and independent of temperature. No drift in the d.c. level of the difference circuit was seen, even though the mean temperature in the fluid was varied more than 10 °C. It was therefore concluded that the difference signal was not affected by temperature variations. This result is in agreement with that of Deardorff & Willis (1967). The sum of the hot-wire outputs is proportional to the longitudinal horizontal velocity, and retains some temperature dependence. The hot wires were calibrated by passing the probe through a stable fluid layer. The speed of traverse and angle of the probe were varied to determine the sensitivity to vertical and longitudinal horizontal velocities. The hot-wire difference was calibrated for 13 velocities between $+10\,\mathrm{cm\,s^{-1}}$ and $-9{\cdot}2\,\mathrm{cm\,s^{-1}}$; it was seen to be nearly linear at $2{\cdot}7\,\mathrm{cm\ s^{-1}\,V^{-1}}$. The r.m.s. deviation from this straight line was $0{\cdot}24\,\mathrm{cm\ s^{-1}}$. The hot-wire sum signal was calibrated at probe speeds of 35·1, 28·3 and 17·9 cm s^{-1} V^{-1}. The calibrations for the three speed differences were within 5% of each other. Two sets of velocity wires were calibrated. Replacement wires were soldered onto the same support, and etched to the same value of resistance (within 2%) as the original one. Considering the nature of the probe and calibration procedure, the absolute accuracy of these velocity measurements is approximately 10%.

A detailed discussion of the characteristics of crossed hot wires is given by Deardorff & Willis (1967). In particular, the contamination of the difference signal by the lateral horizontal velocity is analysed. The present study is primarily concerned with investigating the spectral properties of the vertical velocity and temperature, which are responsible for the turbulent heat transfer. The effect of lateral horizontal velocity is not important for the purposes at hand, and has not been taken into account. Thus the outputs of the difference circuit, the sum circuit, and the temperature circuit, when multiplied by the appropriate calibration factor, will henceforth be referred to as vertical velocity W, horizontal velocity U and temperature T.

The temperature output was unaffected by traverse velocity. Temperature wires were calibrated by changing the mean temperature in an unstable layer and noting the change in system output. Two wires were calibrated, one between $Ra = 1{\cdot}7 \times 10^5$ and $2{\cdot}6 \times 10^5$, with $d = 8$ cm, the other between $Ra = 3{\cdot}2 \times 10^5$ and $4{\cdot}1 \times 10^5$, with $d = 10$ cm. In each case, 13 traverses were made through the layer. In the former case, the r.m.s. deviation of individual traverses was 0·2 °C and the change in mean temperature was 1·8 °C. In the latter the r.m.s. deviation was 0·1 °C and the mean temperature change was 0·7 °C. The mean of these two calibrations was used in calculating results presented in §4. Thus the absolute accuracy of this calibration is approximately 10%.

Output signals for W, U and T were recorded on a Honeywell FM tape recorder at 30 in. s^{-1} for each traverse. A minimum of 3 min was allowed between traverses for the data of §4, and 10 min for the data of §5. (Section 2 explains these times, and discusses the limitations of the traversing mechanism.) At the end of the experimental period, all the traverses were played back at half-speed (15 in. s^{-1}) into a Pastoriza A/D converter (12 bit resolution), connected to a Digi-Data computer-compatible incremental tape recorder. The process resulted in a sampling rate of 61·5 Hz. The accuracy of this entire system was limited by the FM tape recorder noise and drift, which were less than 5%.

Digital data were processed on the UCLA Campus Computing Network's IBM 360/91 computer. The first 512 points, after the probe traverse had come up to speed, were Fourier analysed by conventional techniques. The length of traverse analysed was thus 2·4 m, roughly in the centre of the convection region. The variance spectra

$$C_{12} = a_1 a_2 + b_1 b_2,$$

where the a's and b's are the cosine and sine coefficients of the Fourier analysis of series 1 and 2, were calculted for U, W and T at each frequency from 0·12 to 30·75 Hz. The results were smoothed,

$$C_{12}(f) = \tfrac{1}{4}C_{12}(f-\Delta f) + \tfrac{1}{2}C_{12}(f) + \tfrac{1}{4}C_{12}(f+\Delta f),$$

in order to reduce truncation effects. The frequencies were converted to wavelengths L by using the speed of the probe.

The data-recording procedure varied slightly during the experimental programme, since the data were used for two purposes. For magnitudes of spectra at different Ra to be comparable, it was essential that the calibration of the entire recording system remained constant. Thus, for the results described in §4, the calibration of the recording system was kept constant, and was checked periodically. However, for investigating the wavelengths of spectral peaks in §5, the magnitudes were not deemed crucial, so the record and playback amplifiers of the FM tape recorder (the only adjustments possible in the entire system) were adjusted to optimize the recorded signal.

An example of the data recorded is shown in figure 1 (*b*). One traverse is shown for $Ra = 2{\cdot}7 \times 10^6$, one for $Ra = 1{\cdot}3 \times 10^7$. The segments shown represent the entire traverse, after the traverse mechanism attained a constant speed. Different values of d were used; they are shown in the figure. Inspection of the traces shows a high correlation between W and T, as expected.

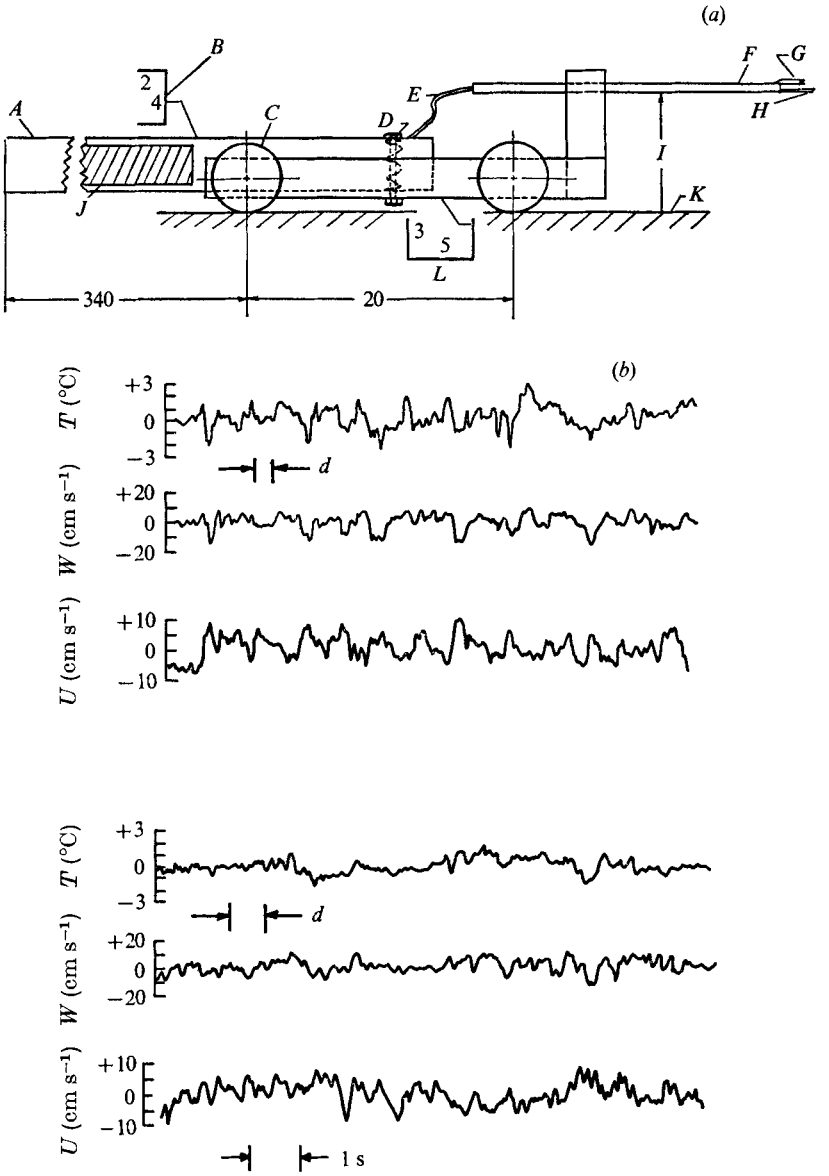

FIGURE 1. (*a*) Probe-traversing mechanism. *A*, friction-drive, constant-speed motor; *B*, support-beam section; *C*, rubber-tired wheels; *D*, spring coupling; *E*, shielded cables; *F*, probe support; *G*, crossed hot wire; *H*, temperature wire; *I*, variable height; *J*, balance weight; *K*, lower plate; *L*, car section. (*b*) Example of sensor outputs. Top: $Ra = 2{\cdot}7 \times 10^6$, $d = 11$ cm, $\Delta T = 31$ °C. Bottom: $Ra = 1{\cdot}3 \times 10^7$, $d = 20{\cdot}8$ cm, $\Delta T = 22$ °C. Traverse taken midway between upper and lower plate. Arrows indicate a time of 1 s, which corresponds to $2{\cdot}6d$ for $d = 11$ cm and $1{\cdot}4d$ for $d = 20{\cdot}8$ cm, using a probe speed of 28·3 cm s^{-1}

2.3. *Limitations of velocity and temperature measurement*

A number of difficulties are apparent in the use of the probe and traverse, described above, to measure temperatures and velocities. The first is the very basic problem of trying to investigate a flow that varies in time and in both horizontal directions by passing a probe along a single line. Another difficulty is the effect of disturbing the flow by introducing a moving probe into the convecting fluid. These difficulties will be discussed in turn in this sub-section. It should be noted at the outset, however, that the measuring technique is standard, having been used by Deardorff & Willis (1967) and Brown (1973) in previous investigations of turbulent convection in air. The technique was chosen because it was the only practical way to obtain information on the horizontal variations of temperature and velocity from the convection apparatus described above.

The turbulent convective flows being investigated vary with time, and the probe takes 8·5 s to traverse the 2·4 m length of traverse, so the results do not represent an instantaneous picture of the motion. For a typical case of $d = 10$ cm, with a predominant horizontal scale of motion (see §4, figure 3) of $6d = 60$ cm, the probe takes approximately 2 s to cross a disturbance. With vertical and horizontal velocities of approximately 10 cm s^{-1} in the turbulent flow, we see that considerable distortion has occurred during the time of traverse across the disturbance. However, it is observed that the time scale for a particular thermal disturbance is greater than d/W. No exact results are available, but experience indicates that the time scale may be of the order of $T = 10d/W$, long enough that the moving probe makes a reasonable estimation of the size of the disturbance.

Another inherent difficulty is that of investigating a three-dimensional flow by passing the probe only along a single line. Even if the disturbances were two-dimensional rolls (which would occur at lower Ra), random orientation relative to the traverse line would cause the wavelength to be overestimated. This deficiency is perhaps the most serious of the present method. With no further information available, we must use the size of elements measured along a line as indicative of their horizontal extent, averaging together a large number of traverses to overcome the problem of orientation.

Because the probe disturbs the flow, we must decide how long to wait between traverses so that thermal and velocity disturbances caused by the probe have decayed sufficiently. In discussing characteristic times in the present experiment, it should be kept in mind that we are dealing with turbulent convection. The appropriate velocity scale is therefore not the conduction velocity k/d, but the convection velocity w_* where

$$\frac{w_*}{k/d} = (Pr\,Ra\,Nu)^{\frac{1}{3}}.$$

This has been shown by Deardorff (1970); and it is shown conclusively by the results presented in §4 (figures 7–9). The characteristic time scale is therefore not d^2/k, but must be the convection time scale

$$\frac{T_{\text{conv}}}{d^2/k} = (Pr\,Ra\,Nu)^{-\frac{1}{3}}.$$

The largest Ra investigated by the above-mentioned traversing mechanism was $Ra = 1{\cdot}7 \times 10^7$ with $d = 24$ cm. For this value of d, we get $d^2/k \sim 50$ min and $T_{\text{conv}} \sim 50$ min/600 $\sim$ 5 s, which is one-half the mean orbital time of a particle in a convection roll when we use the r.m.s. velocity of 7 cm s^{-1}. At lower Ra, disturbances are seen to propagate through convective chambers from one thermal 'cell' to another, so that the appropriate time scale is the mean orbital time times the number of cells (Chen & Whitehead 1968). The author believes that, because the present flows are turbulent, such a time is much too long for the present high Ra case, since the disturbance caused by the probe will be 'mixed up' and dissipated by the turbulent convective velocities. Even so, the minimum of 3 min that was allowed between traverses is greater than this time scale.

The sketch in figure 1 (a) shows that the frontal area of the car that carried the probe through the chamber was approximately 6 cm × 6 cm. At the lowest Ra it fills the entire depth of the layer, but it is less than 2% of the total cross-sectional area of the chamber. When the probe speed is 28 cm s^{-1}, the nearest point of the chamber is equivalent to being 840 body lengths downstream of the car after a waiting time of 3 min. With a Reynolds number of approximately 700, the wake should dissipate by at least a factor of 30, not counting the presence of the top and bottom boundaries and large convective velocities (Schlichting 1960).

As the car moves across the chamber, 240 cm of 2 cm × 4 cm aluminium support beam enters at the temperature of the laboratory. Since the probe support is introduced into the chamber for less than 16 s, and its area of 2880 cm^2 is only 2% of the area of one of the plates, the thermal effect is considered negligible.

Of course, the best way to evaluate the disturbing effect of the traverse car is to test it in operation. Under conditions of neutral and slightly stable thermal boundary conditions, velocities induced by the probe were not noticeable (after stopping the probe abruptly) after 30 s. This agrees with the statement of Deardorff & Willis (1967), that no effect of the probe was noticed for waiting periods of longer than 30 s. More conclusively, the results of spectral analysis of the velocity and temperature signal showed no fixed-frequency spectral peak from one traverse to the next. The dominant horizontal wavelengths shown in §4 were all obtained by averaging together a large number of traverses. In no case did the spectral peaks coincide for different traverses. Since any significant disturbance from the probe mechanism would be expected to appear as the same frequency peak in every traverse, it is concluded that these disturbances were not significant in the present experiment.

The experiments described in §5 below were done first, with waiting times of 10 min. The spectral results showed a large variance of spectral peaks for a number of traverses under the same conditions (r.m.s. deviation $\approx$ mean value). No significant trend was seen as the waiting times were changed between 15 and 1 min. For operational considerations (to allow more traverses to be averaged for given conditions) the waiting time was lowered to 3 min for the experiments described in §4. Again, no trend was seen in the spectral results.

2.4. *Heat flux measurement*

The measurement of heat flux across the plate gap posed a much more difficult problem than had been anticipated. The original method was to measure the flow rate and temperature drop in the water channels of both plates when the mean temperature was kept equal to that of the room. However, the size of the experiment and its design made it impossible to obtain consistent results. The construction of the water flow channels and insulation of the plates was not symmetric, so that the heat losses to the room could not be determined to account for discrepancies between heat lost at the lower boundary and heat gained at the upper boundary. In addition, inhomogeneities in temperature in the manifold supplying water to the flow channels were seen to be nearly as large as the drop along the channels.

The second method to obtain heat flux was to measure the amount of electrical power (from a 20 Ω heater) necessary to keep the lower plate at a constant temperature very close to that of the room. With the lower plate and its supply reservoir at room temperature, the only heat losses are to the upper plate. Heat transfer due to radiation was calculated using

$$q_{\text{rad}} = A(2/\epsilon - 1)^{-1}\sigma(T_2^4 - T_1^4),$$

where the emissivity $\epsilon = 0{\cdot}04$, area $A = 12{\cdot}2\,\text{m}^2$ and the radiation constant $\sigma = 5{\cdot}7 \times 10^{-12}\,\text{W}\,(\text{cm}^2\,\text{K}^4)^{-1}$.

This relation is taken from Jakob (1949); it is the net radiative transfer from one plate to the other, counting all the multiple reflexions from each plate, and assuming that the area of the plates is very large relative to the separation distance d. At large Ra the separation d becomes larger, and the assumption of infinite plates is not so good. However, using the appropriate relations given by Jakob (1957) that take into account the finite extent of the plates and re-radiation by the side walls, it is seen that the results are nearly the same as those given above. When we use the largest value of $d = 180\,\text{cm}$, the shape factor becomes $(2/\epsilon - 0{\cdot}6)^{-1}$ instead of the $(2/\epsilon - 1)^{-1}$ given above. The value of emissivity given is appropriate for 'bright' aluminium at infra-red wavelengths ($9{\cdot}3\,\mu$m at 40 °C). The effect of surface oxidation is unimportant at these wavelengths, since the oxide layer is much thinner than one wavelength.

The amount of heat due to radiation was not large, being less than 10% of the convective transfer for all the cases reported below. Since, after radiation effects are subtracted, heat can be lost from the lower plate only through the fluid to the cold upper plate, this method gives a definite lower bound on the convective heat transport. That is, we know all the heat that left the lower plate went into driving the convective motion. However, we do not know how much heat was conducted through the insulating side walls and also went into driving the motion. The influence of conduction through the side walls is appreciable at large d, and will be discussed below.

This method of determining the heat flux gave encouraging results, but a systematic error was noted in the results. It was seen that at low values of heat flux no electrical power at all was needed to maintain constant temperature in

the lower plate. Evidently, enough mechanical energy was introduced by the flow system (gravity drop from the reservoir and a 480 W centrifugal return pump) to influence the results.

The amount of mechanical energy was found by operating the system at $Ra = 7 \times 10^4$ and noting the equilibrium temperature of the lower plate (0·4 °C above room temperature as measured by the average of 4 thermocouples referenced to a large heat sink at room temperature) with no electrical heat input. The heat losses through the convective fluid and to the room must equal the mechanical input. The convective heat transport was calculated to be 100 W, using the value given by Jakob (1949) for air $Nu = 0{\cdot}21(Ra)^{\frac{1}{4}}$ and the dimensions of the test chamber. All subsequent heat flux determinations, which are reported in § 3, were made at a lower plate temperature of 0·4 °C above room temperature with 100 W added for mechanical heat input.

The experimental procedure was to operate the convection chamber for sufficient time to establish a steady state, then change the electrical power input to the lower plate reservoir until the rate of change of lower plate temperature was zero. Temperatures at the plate supply manifolds were monitored, to see that they had remained constant for at least 15 min. The amount of time required for this process varied, depending on the magnitude of ΔT and the skill of the operator. In nearly all cases, the time to reach equilibrium was between 1 and 4 h. A null method was used to guard against slow changes in room temperature. After a steady state was reached and the power input noted, power was first increased, then decreased slightly, until the plate temperature changed. A power change of 5 % caused the plate temperature to change a noticeable amount, which gave a measure of the relative accuracy of the heat flux determination. The absolute accuracy obviously depends also on the value given by Jakob that was used to determine the mechanical input.

For the largest values of d shown in figure 2 the area of the sides was large enough that appreciable heat was conducted through the styrofoam side walls. In order to estimate the magnitude of this error, the following procedure was used. With $d = 180$ cm the experiment was run twice with 5 cm thick side walls, and then repeated using 10 cm thick side walls. For $d < 180$ cm, the wall thickness was 5 cm. With the 10 cm thick side walls the temperature at the inside wall was measured so that the conduction through the wall could be estimated. Using the conductivity of styrofoam (5 % greater than that of air), and the inside wall temperature measured at the mid-point between the plates, we calculated the loss and compared it with the difference between the results using 5 and 10 cm thick walls. The calculated loss was found to be approximately equal to the difference in heat flux with the two wall thicknesses, and was 13 % of the heat transfer for two different values of ΔT.

Heat loss through the side walls at $d = 180$ cm has therefore been estimated in two independent ways. We can extrapolate that the heat loss remaining with 10 cm wall thickness is approximately the same as the difference between the heat loss at 5 and 10 cm, which is 13 % of the total heat transfer. The loss calculated with temperatures measured at 10 cm lends confidence to this estimate.

At values of d lower than 180 cm, the heat loss through the 5 cm walls should

Quantity	Error (%)	Primary cause
d	± 2	Measurement of d, waviness of plates
ΔT, $\bar{T}$	± 3	Variation across plate
T	± 10	Calibration method, changing wires
U, W	± 10	Calibration method, changing wires
Heat flux, $d \leqslant 24$ cm	± 5	Observed sensitivity
Heat flux, $d = 60$ cm	± 8	Loss through side walls
Heat flux, $d = 180$ cm	± 13	Loss through side walls
Ra	± 10	Accuracy of d
Nu, $d \leqslant 24$ cm	± 10	Measurement of heat flux
Nu, $d \geqslant 60$ cm	± 15	—

TABLE 1

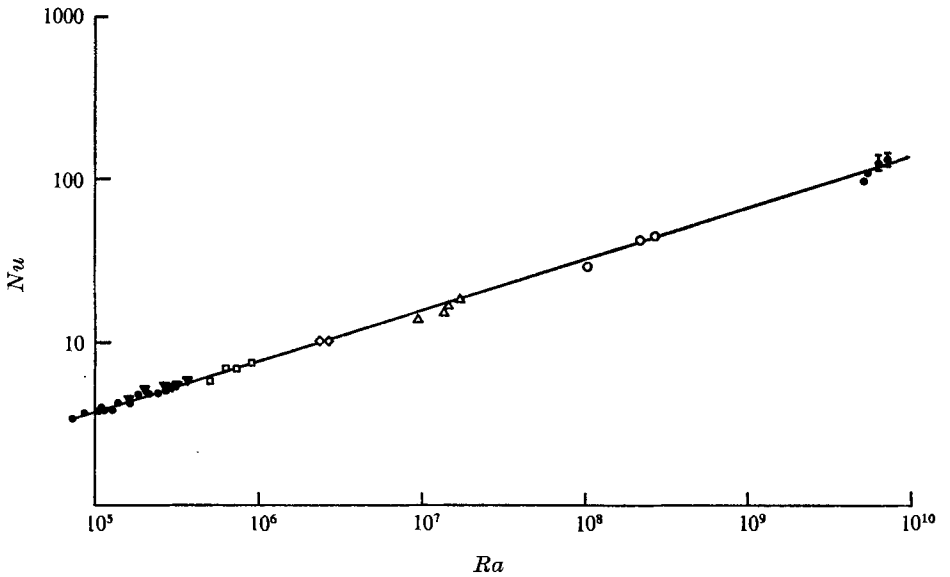

FIGURE 2. Measured heat flux, Nu against Ra. For $d = 180$ cm, lower bar indicates value for 5 cm wall thickness; data point, value for 10 cm wall; and upper bar, calculated loss through walls. Curve fit by eye.

d (cm)	6	8	10	14	24	60	180
	●	▼	□	◇	△	○	⧳

be reduced by $d/180$, since it is proportional to the area of the walls and the mean temperature of the layer $\bar{T}$. Thus the side-wall loss becomes only 8 % of the total heat transfer for the next largest value of $d = 60$ cm, and 3 % for $d = 24$ cm.

2.5. *Summary of experimental errors*

For each of the quantities that were determined experimentally, the expected errors have been given above. They are collected in table 1, along with the derived quantities. As noted above, the relative error in U, W and T is 5 % for the results described in §4.

3. Heat flux measurement

Given in figure 2 are the results of heat flux measurements by the method outlined above. The Nusselt number Nu, defined as the ratio between total heat transport and that due to conduction alone, is given against Ra for

$$7{\cdot}0 \times 10^4 < Ra < 7{\cdot}4 \times 10^9.$$

We calculated the conductive heat transfer using the air conductivity at the mean temperature of the two plates. For $d = 180$ cm, the 5 cm wall results are shown as the lower bar, and the 10 cm wall results are shown as the data points. The upper bar includes the estimated heat loss through the walls. The results for $d = 180$ cm should be used with caution, since, at such a low aspect ratio ($L/d = 2$), even a small amount of heat applied over the side boundaries could significantly affect the flow.

Within the scatter inherent in the data, a curve of $Nu = 0{\cdot}13\,Ra^{0{\cdot}30}$ fits well. There is no indication of a change of slope of the curve at high Ra.

4. Temperature and velocity measurement

Keeping in mind the limitations discussed in §2.3, we proceed to discuss horizontal velocity and temperature spectra calculated from traverses through the convection chamber. In figure 3 are the results for the cospectra of velocity and temperature C_{WT} of a large number of traverses at conditions ranging from $Ra = 0{\cdot}4 \times 10^5$ to $Ra = 1{\cdot}7 \times 10^7$. Cospectral density is plotted against the non-dimensional wavelength L/d. At each Ra at least 12 traverses were made (the average being 14). The spectra were calculated for each traverse according to the method outlined in §2, and the cospectra at each wavenumber were averaged together to give the result shown. The calibrations have been included in the cospectra. By using the specific heat c_p, the chamber dimensions, and the appropriate temperatures, the cospectra have been non-dimensionalized so that the Nusselt number is obtained when the values at all wavelengths are summed, i.e.

$$Nu = 1 + \Sigma C_{WT} d/(k\Delta T).$$

The cospectra for $d > 6$ cm have been reduced by the amount of increase in distance between spectral lines due to changing d, so that the results for different values of Ra can be compared. The area under a given segment of the spectral curve indicates the amount of heat flux supplied by that range of wavelengths. The results of figure 3 show that the wavelength band that accounts for the largest contribution to the total heat flux is centred between $L/d = 4$ and $L/d = 6$.

Although there is considerable scatter in the spectra at a given wavelength, the results over a wide range of Ra show a striking similarity. There is a general monotonic decrease in the heat flux for scale sizes smaller than that corresponding to the spectral peak in each case. Peaks in individual spectra can be seen for smaller scale, but when results for a number of different values of Ra are compared, no systematic change or persistence can be seen. It is therefore assumed that the

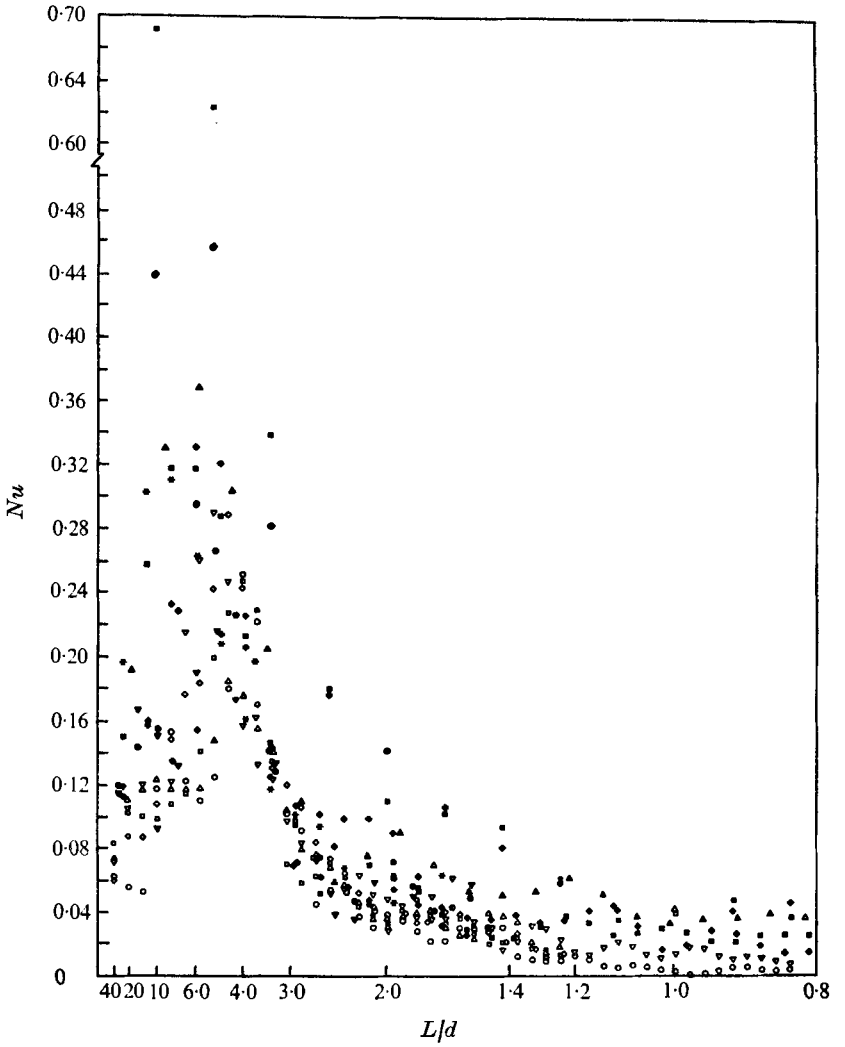

FIGURE 3. W-T cospectral density against wavelength. Value shown is C_{WT} non-dimensionalized such that the sum of C_{WT} at all wavelengths gives the Nusselt number

$$Nu = 1 + \Sigma C_{WT}\, d/(k\Delta T).$$

Ordinate at each L/d is reduced by $\frac{1}{6}d$, so that equal areas under spectral curves represent equal amounts of cospectra, and can be compared for different Ra.

d (cm)	6					8		10				14	24	
Ra ($\times 10^{-5}$)	0·4	0·8	1·2	1·7	2·1	1·7	2·6	3·2	4·1	6·3	8·0	24·0	140·0	170·0
	○	□	△	◇	▽	▼	●	✚	◆	*	×	▲	□	✠

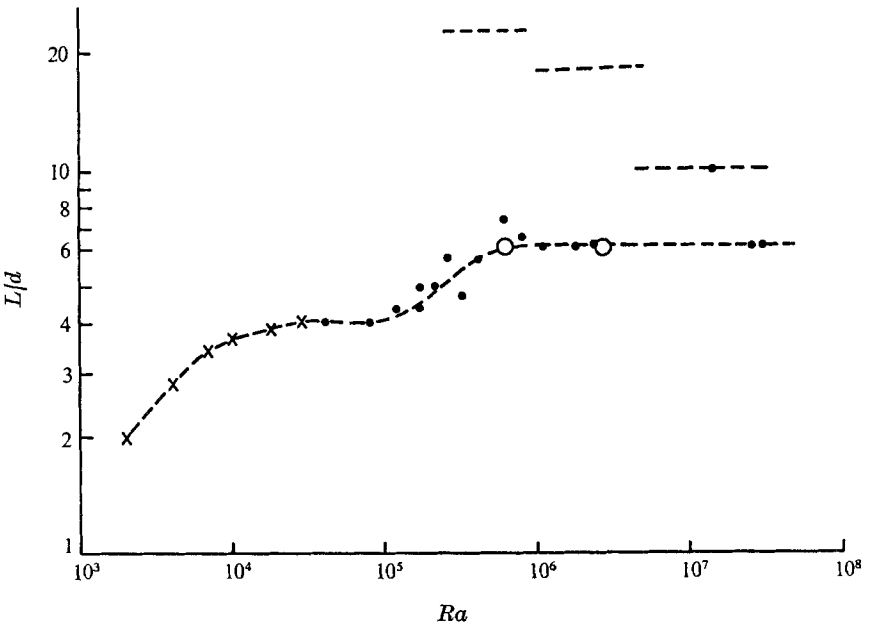

FIGURE 4. Dominant wavelength against Ra. Peak wavelength from figure 3. ●, present experiment, wavelength of maximum C_{WT} from figure 3; ×, Willis & Somerville (1972), from photographs; ○, Deardorff & Willis (1967) from C_{WT}; – – –, limit of Fourier resolution in present experiment.

only significant spectral peak in the heat flux occurs at wavelengths of

$$4 < L/d < 6.$$

The variation of the wavelengths of these spectral peaks with Ra can be seen in figure 4. Also shown are data from Willis & Somerville (1972) for values of Ra less than those obtained in the present experiment, and two points from Deardorff & Willis (1967). We see that the dominant wavelength gradually increases from $L/d = 4$ for $Ra < 10^5$ to $L/d = 6$ for $Ra > 10^6$. In spite of the fact that the limit of resolution shown by the dashed lines is getting close to the dominant wavelength at higher Ra, it appears that the dominant wavelength does not keep growing for $Ra > 10^6$, but remains constant at $L/d = 6$. Another characteristic of the results for $Ra > 10^5$ is the relatively large scatter, which is seen also in figure 3. The region $10^5 < Ra < 10^6$ appears to be a transition region in which the convection changes its scale.

In figure 5 the total cospectra (at all wavelengths) have been used to calculate Nu, which is shown against Ra. The two points shown from Deardorff & Willis were obtained from measured covariance. The r.m.s. variation in the cospectra is shown: it is seen to increase as Ra increases. The slope of the curve of Nu against Ra is close to that obtained in §3, considering the variation that was observed. It should be noted that the variation is characteristic of the present method of obtaining the cospectra: it is seen in the results of Deardorff & Willis (1967) and Brown (1973), who used similar methods.

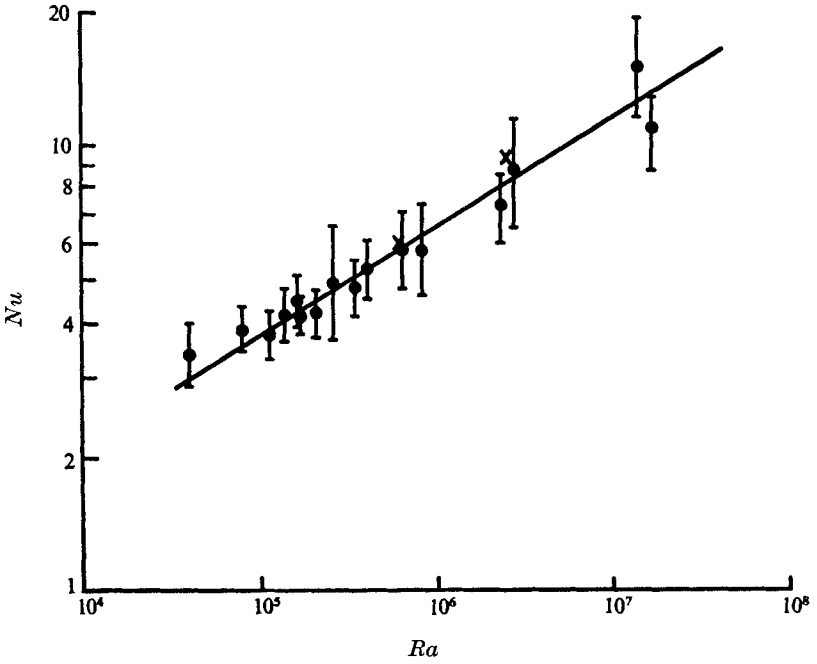

FIGURE 5. Nu against Ra. Nu calculated by summing C_{WT} at all wavelengths. ●, present experiment, bars showing r.m.s. deviation for all transverses at each Ra; ×, Willis & Deardorff (1967).

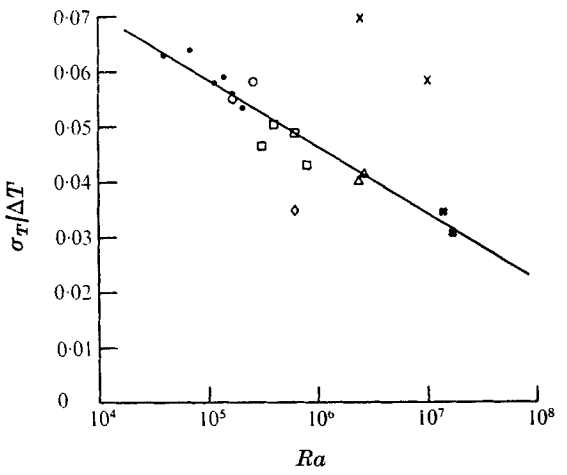

FIGURE 6. The r.m.s. temperature variation against Ra. σ_T scaled by ΔT. ×, Deardorff & Willis (1967); ◇, Thomas & Townsend (1957).

d (cm)	6	8	10	14	24
	●	○	□	△	×

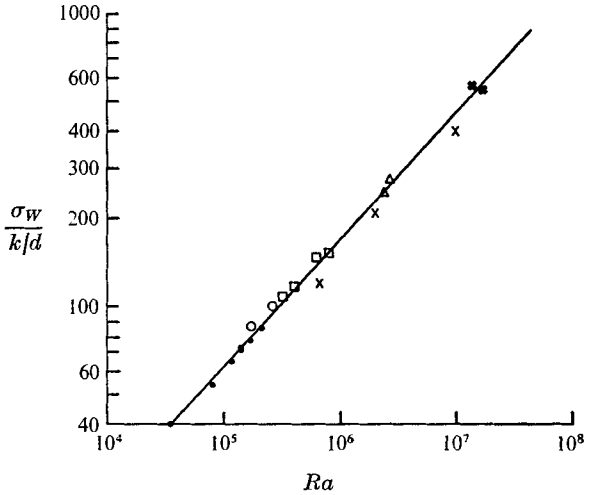

FIGURE 7. The r.m.s. vertical velocity variation against Ra. σ_W scaled by k/d. ——, corresponds to $\sigma_W\,(k/d)^{-1} = 0{\cdot}53\,Ra^{0{\cdot}42}$. Symbols as for figure 6.

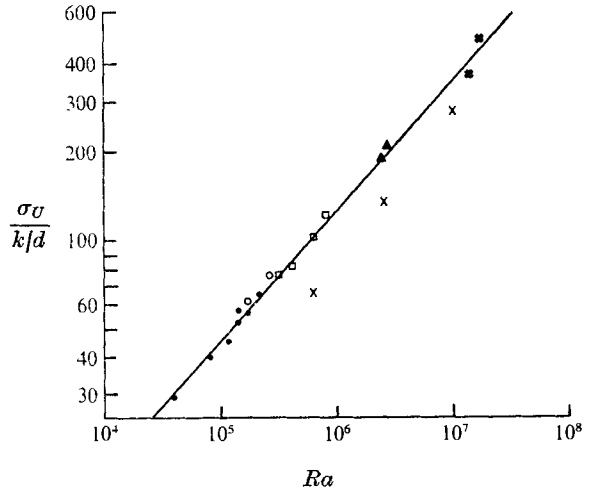

FIGURE 8. The r.m.s. horizontal velocity variation against Ra. σ_U scaled by k/d. ——, corresponds to $\sigma_U\,(k/d)^{-1} = 0{\cdot}29\,Ra^{0{\cdot}44}$. Symbols as for figure 6.

In figures 6–8 the r.m.s. temperature, vertical velocity and horizontal velocity, σ_T, σ_W, σ_U, are shown against Ra, calculated from the same data as the cospectra of figure 3. For comparison with results of previous experiments, both σ_U and σ_W are scaled by the thermal diffusion velocity k/d, and temperature by ΔT. We see a uniform increase in both σ_W and σ_U as Ra is increased. There is no indication of a change in either measured quantity in the range $10^5 < Ra < 10^6$, corresponding to the change in dominant wavelength shown in figure 4. A uniform decrease in σ_T as Ra is increased is also seen, showing no change at $Ra = 10^5$. All of these data are taken at a height halfway between the plates, and give no direct measurements of what may be occurring in the boundary layers near the plates.

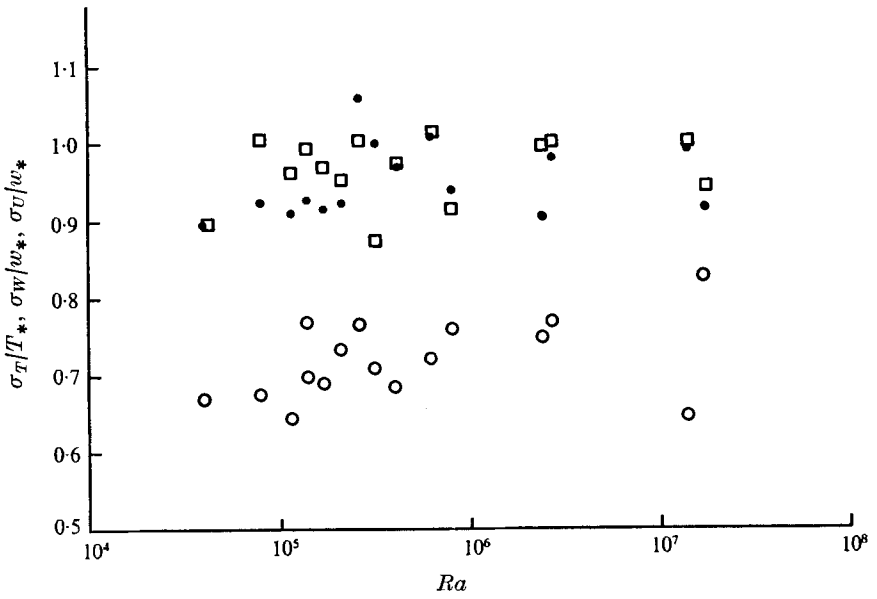

FIGURE 9. The r.m.s. temperature, horizontal and vertical velocity variation against *Ra*. Scaled by $w_* = k/d(Pr\,Ra\,Nu)^{\frac{1}{2}}$, $T_* = \Delta T Nu/(Pr\,Ra\,Nu)^{\frac{1}{2}}$. ●, $-\sigma_W/w_*$; □, σ_T/T^*; ○, σ_U/w_*.

More appropriate scaling parameters are the convective velocity w_* and convective temperature T_* (Deardorff 1970), which can be related to k/d and ΔT by

$$\frac{w_*}{k/d} = (Pr\,Ra\,Nu)^{\frac{1}{3}}, \quad \frac{T_*}{\Delta T} = \frac{Nu}{(Pr\,Ra\,Nu)^{\frac{1}{3}}}.$$

When these scaling parameters are used, the scaled values of σ_W, σ_U, σ_T are nearly independent of *Ra*, as can be seen in figure 9. The value of Nu used to calculate w_*, T_* was obtained from the relation $Nu = 0{\cdot}13\,Ra^{0{\cdot}30}$, shown in figure 2. The mean values of scaled quantities, along with the r.m.s. deviations, are

$$\frac{\sigma_W}{w_*} = 0{\cdot}95 \pm 0{\cdot}05, \quad \frac{\sigma_U}{w_*} = 0{\cdot}72 \pm 0{\cdot}05 \quad \text{and} \quad \frac{\sigma_T}{T_*} = 0{\cdot}98 \pm 0{\cdot}05.$$

5. Structure of horizontal spectra at high *Ra*

In spite of the difficulties inherent in calculating horizontal spectra discussed above, it was desired to search as closely as possible for additional peaks in the spectra. Taking inspiration from the apparent success of Busse (1969) in relating the spectral measurements of Deardorff & Willis (1967) to the multi-α solutions, we decided to force a directional dependence on the experiment by changing the boundary conditions.

Side walls were placed in the chamber so that the dimension normal to the traverse line b was reduced. The transverse aspect ratio b/d was kept equal to 5,

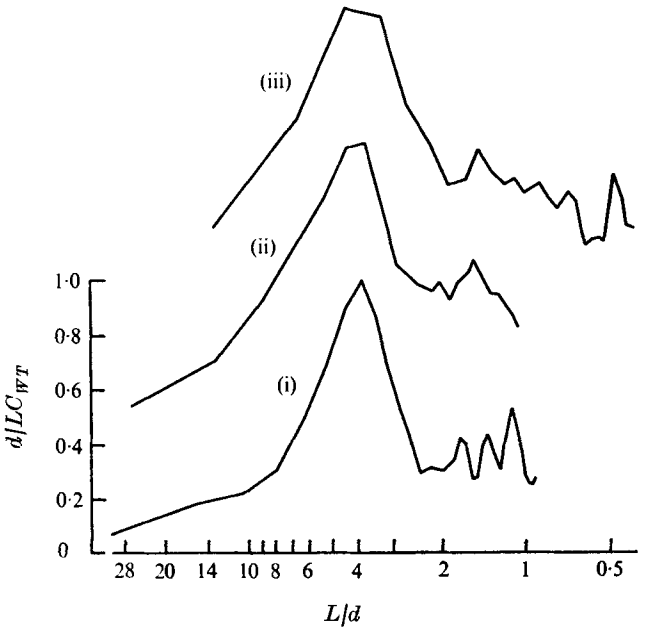

FIGURE 10. Normalized W-T cospectra against L/d, entire chamber. $C_{WT}d/L$ plotted against log (d/L), so that equal areas represent equal amounts of cospectra. $C_{WT}d/L$ normalized to peak value. Curves separated for clarity.

	(i)	(ii)	(iii)
d (cm)	7·6	9·0	18·0
Ra ($\times 10^{-6}$)	1·1	1·8	14·0

as d was changed to vary Ra. This value was believed to be a reasonable compromise between forcing directionality and retaining the important features of the flow. Since the spectral maximum of convection with no side walls occurs at $L/d = 6$ with large Ra, choosing the aspect ratio less than 5 would yield results that could not be generalized to the problem in an unbounded layer.

The operational procedures for the measurement of horizontal variations of velocity and temperature were changed only slightly from those used for the results shown in §4; a delay time of 10 min was used, and the tape recorder gain was altered as described in §2.

We shall restrict ourselves to consideration of the W-T cospectra C_{WT}. Decreasing the aspect ratio changes the other spectral quantities, of course, but the effects can be investigated by considering only C_{WT}. Shown in figures 10 and 11 are C_{WT} for both cases, with the convection including the entire chamber in figure 10 and with an aspect ratio of 5 in figure 11. The values of C_{WT} have been weighted by the inverse of the measured wavelength L/d and plotted with d/LC_{WT} against $\log d/L$, so that equal areas under the spectral curve represent equal amounts of cospectra. The magnitudes have been normalized to the peak value, and separated so that the spectral differences can be examined.

We see in figure 10 that the band of wavelengths $3 < L/d < 6$ contributes the most heat flux, as was indicated by the results in figure 3. The curves for the three

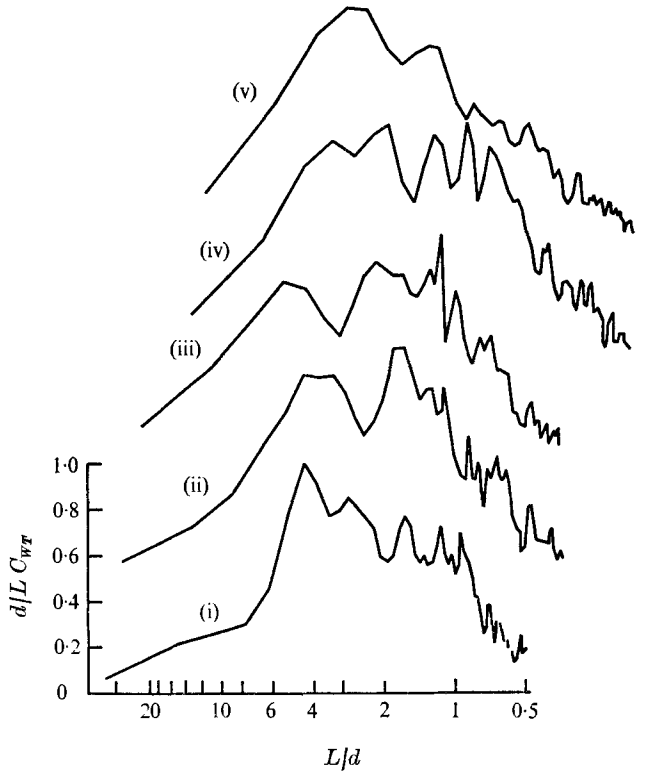

FIGURE 11. Normalized W-T cospectra against L/d, transverse aspect ratio 5. Same as figure 10, except width of chamber reduced to achieve desired aspect ratio

	(i)	(ii)	(iii)	(iv)	(v)
d (cm)	7·6	9·0	11·0	17·0	21·0
Ra ($\times 10^{-6}$)	7·1	1·8	2·6	13·0	21·0

values of Ra are quite similar. When the side walls are introduced so that the aspect ratio is 5, as seen in figure 11, the spectra are significantly altered. A much larger percentage of the total cospectra now is due to smaller sizes $L/d < 3$. These results are very similar to those of Deardorff & Willis (1967). The purpose of introducing side walls was to cause disturbances to line up normal to the traverse. We shall proceed to examine the cospectra at different Ra, looking for some systematic variation that indicates disturbances are being aligned.

We see that there are definite differences between the cospectra from different Rayleigh numbers. However, even though a number of traverses were averaged together in the data shown in figure 11, a large amount of variance exists in the individual peaks of cospectra that are evident. The spectra for individual traverses used to obtain figure 11 show that r.m.s. deviation at a particular wavenumber is nearly equal to the mean, reflecting the fact that the mean value shown is made up of very large values and very small values taken together. The large variance at a particular wavelength causes difficulty in determining the dependence upon the Rayleigh number.

In order to minimize the effect of the large variance in the magnitude of the

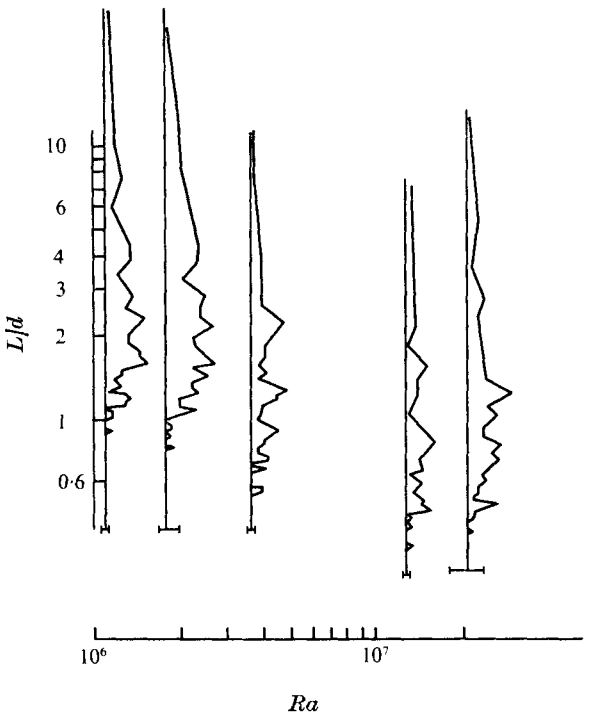

FIGURE 12. Histograms of number of W-T cospectral peaks against wavelength of 5 values of Ra. Range of Ra covered in each histogram is shown at bottom. Total number of spectral peaks is, from left to right, 188, 270, 124, 114, 187.

spectra at different wavelengths, we shall consider only the wavelength of the peaks. This method of presenting the spectral data is shown in figures 12 and 13. The cospectra of each individual traverse through the chamber were scanned to find the wavelength of the three largest maxima. A histogram was prepared for each Rayleigh number, showing the number of spectral peaks observed at each wavelength. In figure 12 only those data are shown for which there were a large number of points, so that the general trend is more evident. Since the wavelengths are shown on a logarithmic scale, the number of peaks at each wavelength has been weighted with d/L, so that equal areas under the curve represent equal numbers of peaks. The number of peaks used at each Rayleigh number is given in the caption. The band of Rayleigh numbers included in each set of data is shown at the bottom of each curve. The trend of decreasing wavelength with increasing Rayleigh number is clearly evident. In each histogram of figure 12, at least three dominant wavelengths can be seen that appear to decrease with the increase in Rayleigh number. However, one should use caution when looking for similarities between curves for which the statistical significance cannot be demonstrated. When all the data are included (figure 13), the trend is not so clear.

The medians of each of the histograms of figure 13 are shown in figure 14, with the size of the plotted point indicating the number of peaks used in each case. A least-squares fit that weights the points according the number of peaks is shown,

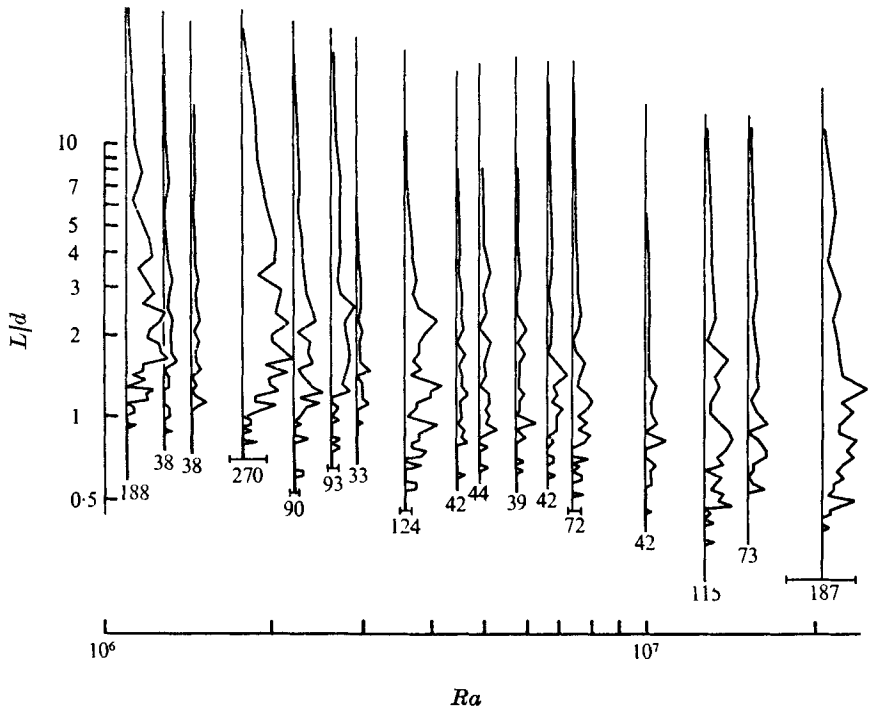

FIGURE 13. Histograms of number of W-R cospectral peaks against wavelength. Same as figure 12, except for all the data obtained.

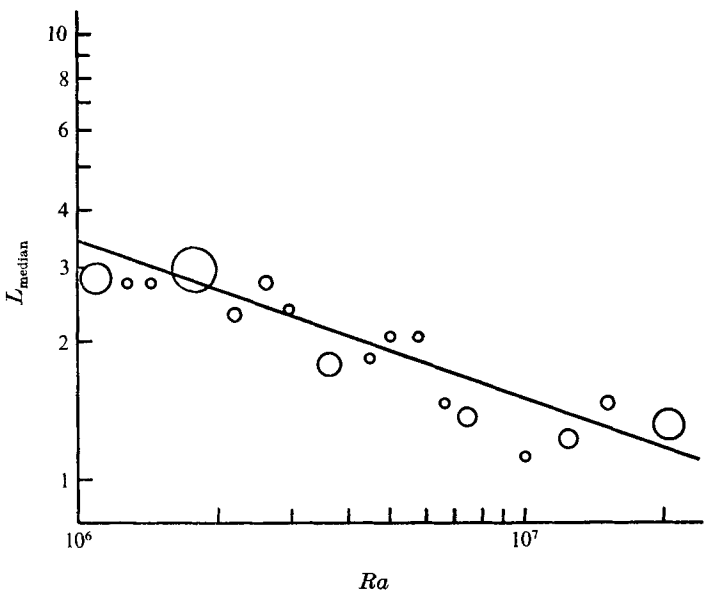

FIGURE 14. Median spectral peak wavelength against Ra. Median wavelength from figure 13. Size of point indicates number of peaks used. Weighted least-squares curve shown is $L_{\text{median}} = 3{\cdot}4Ra^{-0{\cdot}35}$.

and gives $L_{\text{median}} = 3{\cdot}4\,Ra^{-0{\cdot}35}$. The decreasing trend of wavelength with Rayleigh number that is seen in these results is in contrast to the results obtained above and shown in figure 4.

6. Discussion of results

As mentioned in § 1, the problem of thermal convection has been the subject of experimental and theoretical investigation by numerous authors. As the work has progressed, understanding of the phenomenon and its applications has gradually increased. At the same time, however, a number of controversies and inconsistencies have arisen that deserve clarification

One question, resulting from the work of Malkus (1954*a*), involves the discontinuities in heat flux observed experimentally. These discontinuities have been investigated experimentally by Willis & Deardorff (1967), Krishnamurti (1970), Brown (1973) and theoretically by Busse (1967), among others. The transitions have been linked to important changes in the character of the motion and have thus been invaluable in clarifying the evolution to more complicated flows. For example, the second transition (the first transition is the onset of convection) has been linked to the onset of three-dimensional or bimodal convection, and the third transition to time-dependent motions. The transitions have been shown to be highly dependent on Prandtl number, which indicates the importance of the inertial terms. For convection in air, Willis & Deardorff (1967) and Brown (1973) showed that the second transition occurs at $Ra_{t_2} \approx 26\,000$, and that the transition does not depend on whether the depth or temperature drop of the convection box is varied.

Flow changes corresponding to these heat flux transitions were reported by Carroll (1971), who used a stationary temperature probe. In addition to these transitions, he also found significant flow changes at two additional values of $Ra < Ra_{t_3}$. Although this may suggest that heat flux transitions are not the best indicators of changes in the flow, we anticipate that only the most significant flow changes will result in changes in heat flux. The important thing to note is that all the above-mentioned heat flux transitions do accompany a definite change in the fluid flow.

Malkus (1954*a*), Willis & Deardorff (1967) and Chu & Goldstein (1973) indicated the presence of transitions at much higher Ra than Ra_{t_3}. Unfortunately there appear to be no explanations that can relate the onset of these transitions to observable changes in the flow. In the present experiment, none of these heat flux transitions for $Ra > Ra_{t_3}$ can be seen. As discussed in § 2, the limited accuracy of these heat flux measurements results in too much scatter to see such changes. Examination of the spectral data of § 4 reveals no observable difference relating to any of the transitions that were observed by the other authors.

It therefore remains to be seen whether these transitions relate to changes in the flow, or are merely artifacts of the experimental configuration. In the experiment of Chu & Goldstein, the small aspect ratio seems an obvious factor. At high Ra their aspect ratios are as low as 1·5, so that the observed transitions may be adjustment of the horizontal wavelength as the temperature is increased.

Since the results of §4 indicate that a large amount of the heat flux is due to horizontal scales several times larger than the depth, application of their results to an unbounded layer is questionable. Aspect ratios in the experiment of Willis & Deardorff were much larger, and are thus more difficult to explain. In any case, the transitions at higher Ra are of limited usefulness, if they cannot be related to flow changes.

A much more easily observed heat flux transition, where the slope change can be noticed on a log–log plot, was seen by Malkus to occur at $Ra \sim 5 \times 10^5$, and is noted in all the studies cited by Jakob (1957). In fact, it is seen in convection in many different geometries, and it is called the transition from 'laminar' to 'turbulent' convection (Jakob 1957). At this value of Ra, Malkus noted an increase in horizontal motions, and Chu & Goldstein observed an increase in horizontal motions near the boundary layer. We see no change in the r.m.s. U velocity as shown in figure 8; but all these observations were made at the mid-point of the layer, not near the boundary. This transition coincides with the value of Ra at which a definite change occurs in the dominant wavelength (figure 4). It is inferred, therefore, that it accompanies a change in the flow, and is distinct from the series of high Ra transitions observed by Willis & Deardorff and Chu & Goldstein. While the present study is limited by the lack of information about the two-dimensional extent of the convection patterns as has been noted above, it appears that the transition at $Ra \sim 10^5$ coincides with the development of a collective or spoke-pattern instability (Busse & Whitehead 1974).

This instability has been observed in convection of silicon oil, and results in centres that are semi-permanent and characterized by predominant upflow or downflow. The wavelength between these centres is of the order of $L/d = 6$ or larger, and the centres exist as the most persistent features in a generally time-variant flow. Such persistent features would be naturally singled out by the present method of averaging spectra. The dependence on Pr precludes any direct comparison with the value of Ra at which the instability occurs. It can be seen in figure 4 that the apparent transition occurs in the range $10^5 < Ra < 10^6$ for convection in air. This value of Ra is of approximately the same magnitude as that for the high Pr silicon oil, although the comparison is only a rough one. Although the data shown in figure 4 are limited at large Ra by the Fourier resolution in the convection chamber, the results indicate that the predominant wavelength remains constant after the transition.

The most important result of this study is the observation of definite measurable changes in the flow corresponding to the collective instability. The tendency of the flow, even in the seemingly turbulent flow at high Ra, towards subharmonic or larger scale response is characteristic of convection, which holds implications for a wide variety of applications. The similarity to dry convection in the unstable planetary boundary layer is quite apparent. Deardorff (1970) showed that, when scaled by w_* and T_*, the measurements in closed convection-box experiments are similar to those in the unstable atmosphere taken above the level given by the Monin–Oboukhov scale height, which describes the limit of shear-dominated motion. The present results indicate that horizontal scales of motion several times larger than the depth of the convecting layer are very important in trans-

porting heat. The importance of these scales of motion is indicated by the results of Deardorff & Willis (1967) using a configuration similar to the present one. Carroll (1971) has Fourier-analysed a fixed array of temperature probes and also obtained results that suggest the importance of motions larger than the layer depth. The existence of large-scale disturbances was noted by Willis & Deardorff (1974), and used to explain discrepancies between their experimental results (made in a chamber of aspect ratio 1·5) and aircraft measurements in the atmosphere. Similarity of the present results to other observed atmospheric convection (such as cellular cloud patterns) is less direct, but the tendency towards large horizontal scales is present. This tendency is also observed in turbulence without convection, in many cases.

The results for σ_T given in figure 6 show a systematic and rather large discrepancy when compared with the results of Deardorff & Willis (1967). Values of Nu shown in figure 5 are close to those of Deardorff & Willis, but the variance is so great that comparison is difficult. The values of σ_W and σ_U shown in figures 7 and 8 are closer to Deardorff & Willis's results than σ_T. In looking for differences between the two studies to try to account for the different results, the larger aspect ratio of the present work is an obvious candidate. However, the lack of any systematic trend in σ_T, σ_W and σ_U suggests the effect is not important. Correlation coefficients for the present results compare well with those measured by Deardorff & Willis at mid-level. For example, the present results give

$$r_{WT} = \frac{C_{WT}}{(C_{WW}C_{TT})^{\frac{1}{2}}} = 0{\cdot}51 \quad \text{for} \quad Ra = 6{\cdot}3 \times 10^5 \quad \text{and} \quad d = 10\,\text{cm},$$

compared with $r_{WT} = 0{\cdot}61$ given by Deardorff & Willis.

No reason is known for the large σ_T discrepancy. The temperature calibration discussed in § 2 is believed to be accurate to $\pm 10\,\%$, but the results of Deardorff & Willis are 60 % higher than the present ones. The latter yield $\sigma_T/T_* = 1{\cdot}0 \pm 0{\cdot}05$, which appears to be close to comparable measurements in the real and simulated planetary boundary layer (Willis & Deardorff 1974) at the level of maximum σ_W.

As stated in § 1 there are two ways of approaching convective turbulence. Either we proceed step by step through the sequence of instabilities, which lead to the complex flow we designate as turbulence, or we search for structures in the fully-turbulent flow that can be related to some physical model. In § 5 we attempted the latter approach, changing the boundary conditions to overcome limitations in the measuring technique. It was hoped that lowering the aspect ratio in one direction would make possible determination of smaller-wavelength disturbances lost in the averaging process. The goal was to relate these wavelengths to a reasonable model, the prime candidate being analyses based on Malkus's suggestion of maximizing the turbulent transport. In order to relate the measurements to the results of these theories, a brief digression is necessary into the nature of multi-α solutions. The reader is referred to Busse (1969) for a complete description of the solutions.

The multi-α solutions are multiple boundary-layer solutions to the variational problem of maximal heat flux across the gap. As we move from the interior

towards the boundary, each succeeding boundary layer has a vertical scale one-quarter of that of the preceding one, and a particular horizontal scale of wavenumber α that decreases as the Rayleigh number is increased. The number of boundary layers present at a particular Rayleigh number is determined by maximizing the total heat flux. The horizontal spectra in the centre of the convection layer correspond to the horizontal scale of the outermost boundary layer, which dominates the interior region. The predominant horizontal wavelength in the interior should therefore decrease as $Ra^{-\frac{1}{4}}$ until a transition is reached, at which point a new and larger horizontal scale becomes predominant, corresponding to the next larger wavelength. The horizontal scale of the new boundary layer should in turn decrease as the Rayleigh number is increased further. However, since there is not much difference between the amounts of heat flux due to the first few boundary layers near the interior, the flow cannot be expected to show a strong preference for one rather than another. Thus, we expect that the dominant horizontal scale would alternate between the preferred and the next smaller if the bounding solutions were representative of the actual flow.

The results of §5 do not lead to a definite confirmation or refutation of the above hypothesis. Comparison of figures 10 and 11 indicates that lowering the transverse aspect ratio did indeed increase the amount of cospectra due to smaller wavelengths. But distinct spectral peaks that have a systematic variation with Ra cannot be discerned. The histograms of figures 12 and 13 indicate that the number of peaks at smaller wavelength increases as Ra increases, and this is confirmed in figure 14. However, this result is a long way from positive evidence for the existence of multi-α type structures in the flow.

The results in figure 4, which use the entire convection chamber, indicate that the dominant wavelength increases with Ra, in contradiction to the multi-α bounding solutions and the results of §5. Until it is possible to make a better determination of the horizontal structure than does present instrumentation, the effects of decreasing the transverse aspect ratio will be in question. It is clear, however, that the spectral results of Deardorff & Willis, taken at low aspect ratio, are not applicable to the case of large aspect ratio since they resemble the results in figure 11 more than those in figures 3 and 10.

Perhaps the equivocal nature of the results regarding structures in the flow are just due to the inadequacy of the available velocity and temperature data. It seems more likely to the author, however, that they do convey important information: i.e. that the upper bounding solutions are just useful as a viewpoint or way of looking at turbulence, and should not be taken as solutions of the motion. Indeed, both Howard (1963) and Busse (1969) caution that their solutions are only for the bounding problem, not necessarily for the flow. Perhaps the variational problem needs constraints, in addition to those on energy and continuity. Or, more basically, perhaps the idea of maximal turbulent transport is true only in some average sense, and is not a good way to arrive at solutions of the motion. The spectral data of this study all show that vertical velocity and temperature are not perfectly correlated, as would be the case with optimal heat transport. The maximum coherence, which occurs at the peak wavelength in the cospectra, is approximately 0·7.

Heat flux measurements do not offer proof of multi-α type motions. The bounding solutions indicate that $Nu \sim Ra^{\frac{1}{2}}$ at large Ra. An analysis by Kraichnan (1962) also suggests this dependence at large enough Ra is due to increased velocities near the boundary layer because of the large-scale convection. Such dependence is in contrast to the $Nu \sim Ra^{\frac{1}{3}}$ dependence obtained from similarity arguments, which allow the length scale d to cancel out. We see from figure 2, that, in the range of these experiments, $Nu = 0{\cdot}13\,Ra^{0{\cdot}30}$ for $Ra < 10^{10}$. The present results therefore show no enhancement over the $R^{\frac{1}{3}}$ similarity dependence. Since Kraichnan indicates that the enhancement of Nu should not occur until $Ra \sim 10^{24}$, which is clearly beyond the range of experiment, we can only say that, if such enhancement occurs, it must be at higher Ra than we can attain. It should be noted that the functional dependence is $Ra^{0{\cdot}30}$, instead of the $Ra^{\frac{1}{3}}$ that would be true if the length scale cancelled. Other heat flux measurements (Goldstein & Chu 1969) have obtained the same result (i.e. that Nu increases less rapidly than $Ra^{\frac{1}{3}}$). It appears that the flow near the lower boundary is effected by large-scale motions from outside the boundary layer, but with the effect of hindering, not enhancing, the heat flux. Such hindrance seems plausible, since large-scale downdrafts near the lower boundary can suppress the depth of the boundary layer, thus hindering the growth of small-scale instabilities that enhance the heat flux. Large-scale horizontal velocities could also limit the heat flux by breaking up ordered structures in the turbulent flow.

The author gratefully acknowledges the suggestions and support of Professor F. H. Busse in completion of this work. The assistance of P. K. Amar at the outset of the experimental work is greatly appreciated. The convection chamber was designed by J. A. Whitehead, and built by the late P. A. Cox. This work was supported by the National Science Foundation under grants GA 31247 and GA 43063. The work was completed and revised at the Wave Propagation Laboratory, National Oceanic and Atmospheric Administration, with the support of the National Research Council.

REFERENCES

Blackwelder, R. F. & Kovasznay, L. S. G. 1972 Time scales and correlations in a turbulent boundary layer. *Phys. Fluids*, **15**, 1545–1554.

Browand, F. K. & Winant, C. D. 1973 Laboratory observations of shear-layer instability in a stratified fluid. *Boundary-Layer Met.* **5**, 67–78.

Brown, W. S. 1973 Heat-flux transitions at low Rayleigh number. *J. Fluid Mech.* **60**, 539–559.

Busse, F. H. 1967 On the stability of two-dimensional convection in a layer heated from below. *J. Math. & Phys.* **46**, 140–179.

Busse, F. H. 1969 On Howard's upper bound for heat transport by turbulent convection. *J. Fluid Mech.* **37**, 457–477.

Busse, F. H. & Whitehead, J. A. 1974 Oscillatory and collective instabilities in large Rayleigh number convection. *J. Fluid Mech.* **66**, 67–79.

Carroll, J. J. 1971 The structure of turbulent convection. Ph.D. dissertation, Department of Meteorology, U.C.L.A.

CHEN, M. M. & WHITEHEAD, J. A. 1968 Evolution of two-dimensional periodic Rayleigh convection cells of arbitrary wavenumbers. *J. Fluid Mech.* **31**, 1–15.

CHU, T. Y. & GOLDSTEIN, R. J. 1973 Turbulent convection in a horizontal layer of water. *J. Fluid Mech.* **60**, 141–159.

DEARDORFF, J. W. 1970 Convective velocity and temperature scales for the unstable planetary boundary layer and for Rayleigh convection. *J. Atmos. Sci.* **27**, 1211–1213.

DEARDORFF, J. W. & WILLIS, G. E. 1967 Investigation of turbulent thermal convection between horizontal plates. *J. Fluid Mech.* **28**, 675–704.

GOLDSTEIN, R. J. & CHU, T. Y. 1969 Thermal convection in a horizontal layer of air. *Prog. Heat and Mass. Trans.* vol. 2, pp. 55–75. Pergamon.

HOWARD, L. N. 1963 Heat transport by turbulent convection. *J. Fluid Mech.* **17**, 405–432.

JAKOB, M. 1949 *Heat Transfer*, vol. 1. Wiley.

JAKOB, M. 1957 *Heat Transfer*, vol. 2. Wiley.

KRAICHNAN, R. H. 1962 Turbulent thermal convection at arbitrary Prandtl number. *Phys. Fluids*, **5**, 1374–1389.

KRISHNAMURTI, R. 1970 On the transition to turbulent convection. Part 1. The transition from two- to three-dimensional flow. *J. Fluid Mech.* **42**, 295–307.

MALKUS, W. V. R. 1954*a* Discrete transitions in turbulent convection. *Proc. Roy. Soc.* A **225**, 185–195.

MALKUS, W. V. R. 1954*b* Heat transport and spectrum of thermal turbulence. *Proc. Roy. Soc.* A **225**, 196–212.

SCHLICHTING, H. 1960 *Boundary-layer Theory*, 4th edn. McGraw-Hill.

THOMAS, D. B. & TOWNSEND, A. A. 1957 Turbulent convection over a heated horizontal surface. *J. Fluid Mech.* **2**, 473–492.

WILLIS, G. E. & DEARDORFF, J. W. 1967 Confirmation and renumbering of the discrete heat-flux transitions Malkus. *Phys. Fluids*, **10**, 1861–1866.

WILLIS, G. E. & DEARDORFF, J. W. 1974 A laboratory model of the unstable planetary boundary layer. *J. Atmos. Sci.* **31**, 1297–1307.

WILLIS, G. E. & SOMERVILLE, R. C. J. 1972 Roll-diameter dependence in Rayleigh convection and its effect upon the heat flux. *J. Fluid Mech.* **54**, 351–367